Force Sensing Interventional Radiology Device

A Technical Report submitted to the Department of Biomedical Engineering

Presented to the Faculty of the School of Engineering and Applied Science

University of Virginia • Charlottesville, Virginia

In Partial Fulfillment of the Requirements for the Degree

Bachelor of Science, School of Engineering

Gabriella Ann Grillo

Spring, 2021.

Technical Project Team Members

Sydney DeCleene

Sruthi Gopinathan

On my honor as a University Student, I have neither given nor received unauthorized aid on this assignment as defined by the Honor Guidelines for Thesis-Related Assignments

John Angle, Department of Vascular and Interventional Radiology

Force Sensing Interventional Radiology Device

By

Sydney DeCleene, Undergraduate Department of Biomedical Engineering
Sruthi Gopinathan, Undergraduate Department of Biomedical Engineering
Gabriella Grillo, Undergraduate Department of Biomedical Engineering
John Angle, M.D., Department of Vascular and Interventional Radiology

Word Count: 3576
Number of Figures: 8
Number of Tables: 0
Number of Equations: 1
Number of Supplements: 9
Number of References: 25

Approved: John T. Angle, M.D. Date: 5/7/2021

John Angle, M.D., Department of Vascular and Interventional Radiology

Force Sensing Interventional Radiology Device

Sydney E. DeCleene[a,1], Sruthi Gopinathan[a,1], Gabriella A. Grillo[a,1], John F. Angle, MD[b]

[a] Biomedical Engineering, University of Virginia
[b] Vascular and Interventional Radiology, University of Virginia
[1] Corresponding authors: sd5dh@virginia.edu; sg4wc@virginia.edu; gag5ua@virginia.edu

Abstract

In Interventional Radiology (IR), minimally invasive procedures are conducted by traversing a patient's vasculature via a small incision site. Because minimally invasive (MI) procedures rely on understanding haptic feedback, inexperienced surgeons cannot numerically confirm the amount of force that they are using which could lead to vessel rupture. The goal of this project was to develop a force sensing resistor (FSR) that could be attached to commercially available IR devices to provide IR surgeons with numerical feedback on how much force they are applying. To accomplish this aim, we created a thru-mode FSR made out of copper tape and velostat. Testing the thru-mode FSR alone using a voltage divider circuit showed that the FSR was able produce changes in voltage in response to different forces in its linear range. The FSR was also able to output distinct voltage differences in response to safe force values (0.4-0.6 N) and dangerous force values (5.1-8.9 N). Attaching the FSR to a Cook Aortic Endograft, an IR tool, did not hinder the FSR's ability to detect changes in force. To determine if the FSR was able to measure forces in a vessel-like structure, we modeled and 3D printed a phantom of the abdominal aorta (AA) and common iliac arteries (CIA) out of Elastin 50A resin. The FSR was capable of detecting force changes in the phantom. Lastly, we compared our FSR to a commercially available FlexiForce sensor and determined that there was a statistically significant difference in the voltage outputs (p value = 0.000137) and force readings (p value = 0.007) between the two sensors. Our FSR was more sensitive and cost efficient than the FlexiForce sensor. Our results validate the ability of our FSR to measure force and confirm its potential for use in minimally invasive procedures.

Keywords: Interventional Radiology, educational tool, force sensing resistor, vessel rupture

Introduction

In 2018, the global surgical device market was valued at USD 14.1 billion. The evaluation of this market is expected to grow at a rate of 8.5 percent annually from 2018 to 2026[1]. MI tools are a part of this developing market. MI procedures are beneficial because they do not require a large incision. However, they limit surgeons' visibility which becomes problematic in cases of abnormal patient anatomies. This limited visibility could cause procedure failure.

An interhospital study found that 53 percent of surgical errors were due to inexperience with a procedure[2]. Another study determined that technical errors were the cause of 52 percent of patient injuries[3]. Additionally, 47 percent of MI surgeons reported a significant error in their surgery practices[4]. White et al. suggest that the detachment between visual and haptic feedback in MI surgeries is a main source of surgical error [4]. As seen in Supplemental Fig. 1, when too much longitudinal force is applied to blood vessels they can rupture. The technical error rates in MI surgeries show that there is a need for devices that can train inexperienced operators as well as provide feedback to experienced operators. If surgeons had a better understanding of how external force applications on devices translated to device movements inside the body, patient injury rates due to technical error could be decreased.

Currently, there are no devices being used in a clinical setting that can measure longitudinal force during MI procedures. Though there are multiple devices that have been developed in a research capacity to measure force during surgery, none have been applied to clinical use. Additionally, these devices tend to be highly specialized for a single operator or procedure and do not measure force directly at the vessel wall. For example, in a chest compression study, a glove was created to measure pressure, but the glove had to be customized to each physician's hand and could not be reused by different people for other procedures[5]. The pressure data collected using the glove was also subject to motion artifacts that could have resulted from the fabric moving. Additionally, the glove required a long setup time and this could further delay the already extensive setup time in the operating room. In another study, a wire deflection sensing apparatus was created to measure force in coil embolization of intracranial aneurysms procedures[6]. While this device was operator independent, it was only able to measure the force of a guidewire on a vessel. Larger IR tools such as catheters and endografts are wider and could be more dangerous and in more need of force monitoring.

Our solution is to create a force sensing resistor that is operator independent, can be attached to several IR tools, and can measure force directly at the vessel wall. We intend for this device to be used during MI procedures to reduce patient injury by providing surgeons with feedback on the amount of force that they are using. Our first aim was to design a force sensing resistor that could be attached to any IR tool. Our second aim was to construct two vascular phantoms that could be used to test whether or not our device was capable of measuring force in a structure with similar dimensions and material properties to a vessel.

Materials and Methods:

Force Sensor Materials and Construction

A thru-mode FSR was chosen because it is thin, capable of measuring small forces, and able to produce a linear relationship between force and voltage[7]. To construct our thru-mode FSR we used copper tape, velostat,

and double-sided tape. Copper tape made up the two outermost layers, velostat made up the two middle layers, and double-sided tape was the innermost layer (Supplemental Fig. 2[8]). The copper tape served as the conductive layer and velostat acted as the pressure-sensitive layer. Double-sided tape was used to create a space between the two layers of velostat in order to utilize their pressure-sensing capabilities. These materials were also chosen because of their flexibility and relatively low cost.

For the initial FSR prototypes that were not attached to an IR device, the material layers were cut into square shapes. These standalone FSR prototypes also had thin pieces of copper tape that attached to the copper layer of the sensor and extended off of the sensor (Supplemental Fig. 3). The copper tape extensions were used to connect the sensor to the circuit. For the FSRs built onto an IR tool, the materials were first layered in the same order as the standalone FSRs and were then wrapped around an IR device (Fig. 1). These mounted FSRs also had copper tape extensions to connect to the circuit. In this experiment, the FSRs were attached to a device called a Cook Aortic Endograft, which is commonly used in abdominal aortic aneurysm repair procedures[9].

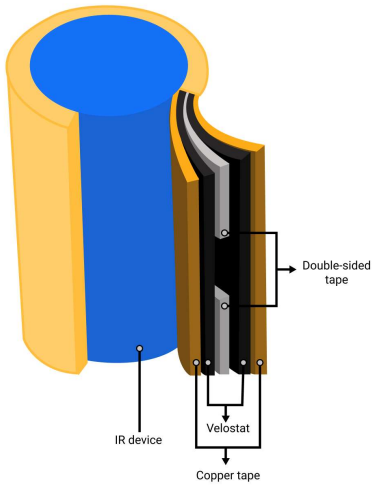

Fig. 1. 3D diagram of our FSR wrapped around an IR device. The copper, velostat, and double-sided tape layers were wrapped around a Cook Aortic Endograft.

Phantom Design and Construction

Using Autodesk Fusion 360, two vascular phantoms were modeled. The first phantom was of the abdominal aorta (AA) and common iliac arteries (CIAs) (Supplemental Fig. 4). Based on literature values, the outer diameters of the AA and CIAs in the phantom were set to be 20.4 mm and 9.91 mm respectively and the vessel lengths were set to 130 mm and 57.76 mm respectively[10–12]. The bifurcation angle between the two CIAs was set to 50.16 degrees[10]. A wall thickness of 2 mm was used for both the AA and CIAs[13]. The second phantom was of the inferior vena cava (IVC) and common iliac veins (CIVs) (Supplemental Fig. 5). Based on literature values, the outer diameters of the IVC and CIVs in the phantom were set to 20 mm and 11.5 mm respectively and the vessel lengths were set to 106 mm and 62.3 mm respectively[14–17]. The bifurcation angle between the two CIVs was set to 42 degrees[18]. A wall thickness of 1.5 mm was used for both the IVC and CIVs[19].

From literature, the tensile strength of the AA and IVC were found to be 1.18 MPa and 2.50 MPa respectively[20,21]. Elastic 50A resin, which has a tensile strength of 1.61 MPa, was the material used to print the AA and CIAs model on a Form 3 SLA printer[22]. The 3D printed AA phantom can be seen in Fig. 2.

Fig. 2. 3D printed phantom of the AA and CIAs. The physiologically accurate dimensions for the phantom were determined from literature. Elastic 50A resin was used to print the phantom.

Circuit Methods

In order to test our thru-mode FSR, we designed a voltage divider circuit. A voltage divider circuit was chosen because of its simple design, low cost, and linear output[23]. We used a 76 Ω resistor as the non-variable resistor in the circuit. This resistor value was chosen based on our initial tests of our FSR's resistance which was measured using a multimeter. The initial tests demonstrated that when large forces were applied, our FSR's resistance decreased to 2 kΩ. From data on other FSRs, we determined that the current through the FSR should be approximately 2.4 mA[23]. Equation 1, where I_{FSR} is the current through the FSR, R_{FSR} is the resistance of the FSR, and V is the voltage, was used to solve for the circuit's non-variable resistor value (R_C).

$$I_{FSR} = \frac{V}{R_C + R_{FSR}} \qquad \text{(Equation 1)}$$

The voltage source was set to 5 V; however, it supplied a voltage of 4.89 V. Solving for R_C with V equal to 4.89 V, I_{FSR} equal to 0.0024 A, and R_{FSR} equal to 2000 Ω yielded a RC of 37.5Ω. We tested the circuit with a few different resistors around the range of 37.5 Ω to see which allowed the circuit to have the highest sensitivity with our FSR. A 76 Ω resistor produced slightly more change in voltage for changes in resistance than the 37.5 Ω resistor. Therefore, a 76 Ω resistor was used for testing. Our circuit is shown in Supplemental Fig. 6. A voltage probe was attached to the copper extension on each end of our FSR in order to determine the change in voltage across the FSR in response to applied force.

Calibration Curve Generation

We created calibration curves for our FSR and a comparative commercial resistor called a FlexiForce sensor. These calibration curves were generated in order to understand how the voltage differences outputted by our sensor relate to applied force and compare to the FlexiForce's voltage outputs. The calibration curves were generated by placing standard weights on the sensors while they were connected to the voltage divider circuit. The voltage across the sensors was recorded for different weight values (20, 50, 100, 150, 200, 250, 500, and 1000 grams). Three trials were performed for each weight value. Calibration of our force sensor on the Cook Aortic Endograft was similar, but consisted of hanging the weights off of the sensor instead of placing them on top of the sensor. This setup is shown in Fig. 3.

Fig. 3. Experimental set-up for measuring the voltage response to force for the FSR attached to a Cook Aortic Endograft. Known weights were hung on the sensor and the voltage output of the FSR was recorded.

Comparison to a Commercial Sensor

In order to determine if there was a statistically significant difference between the force readings outputted by our FSR attached to a Cook Aortic Endograft and a FlexiForce sensor, we applied a constant force to both sensors at the same time. A C-clamp was used in order to apply the same amount of force to both sensors at the same time. This set-up is shown in Fig. 4.

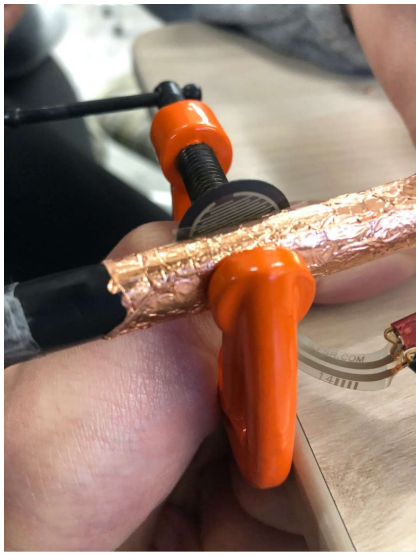

Fig. 4. Experimental setup for measuring a constant force applied to both the FSR on a Cook Aortic Endograft and a FlexiForce sensor. constant force was simultaneously applied to both sensors using a C-clamp and the voltage outputs for both sensors were recorded.

Results:

Proof of Concept

After constructing our initial standalone thru-mode FSRs, we needed to determine if they were able to measure force. The sensors were calibrated using standard weights to determine if there was a relationship present between force and voltage measured across the FSR. Fig. 5 shows this relationship in the sensor's linear reading range. This range contains the expected range of forces for safe operation (0.4-0.6 N)[24].

The sensors were then tested across a wider range to include force values that have been shown to cause vessel rupture (5.1-8.9 N)[25]. This relationship is shown in Supplemental Fig. 7. The voltage response to force relationship over the larger force range was shown to be less linear ($R^2 = 0.6813$) across all three trials. This nonlinearity could be due to the design of the sensor as well as overuse without sufficient recovery time.

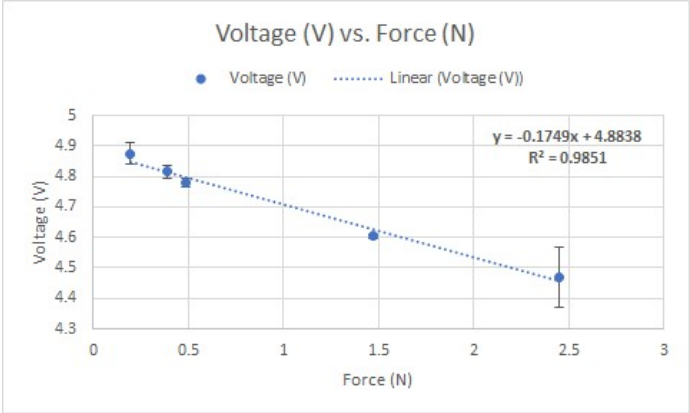

Fig. 5. Voltage versus force calibration curve for a standalone FSR. Known weights were placed on top of the sensor and the voltage outputs were recorded on the y-axis. The curve shows a linear relationship ($R^2 = 0.9851$) between force and voltage.

We constructed the standalone sensor to be flat, which resulted in less space between the layers of the sensor. This limited space reduces the maximum displacement between the layers of velostat. This, in turn, decreases the maximum force the sensor can read. This is because the layers of the sensor are as close as possible at a smaller applied force compared to a sensor with a greater gap between the velostat layers. The sensor was also repeatedly loaded and no time was given to allow the materials of the sensor to recover and return to their original shape. This could cause similar voltage readings to be produced across different force values if the materials are still in their compressed state from the previous trial. Although the relationship between force and voltage is not perfectly linear, there is a distinct difference in voltage between the safe force values and the dangerous force values.

FSR on a Device

Our proof of concept determined that our FSR was capable of measuring force in the correct range. Therefore, we developed a similar FSR that could be placed on an IR device. After attempting to add a sensor to several small catheters, we decided to attach our FSR to a Cook Aortic Endograft (Supplemental Fig. 8). This device has a larger diameter compared to other IR tools and thus is more prone to causing vessel rupture. Additionally, the large diameter was more suitable for the size of our early-stage prototyped FSR.

A calibration curve was generated for the sensor wrapped around the Cook Aortic Endograft. The determined relationship between force and voltage across the FSR is shown in Fig. 6. From Fig. 6, it can be seen that our FSR, when attached to an IR device, has a linear relationship between force and voltage across both safe and unsafe force levels. This indicates that the FSR attached to an IR tool can detect the difference between safe and unsafe forces. We suspect that wrapping the FSR around the device produced better linearity ($R^2 = 0.9817$) compared to the sensor laying flat on a surface ($R^2 = 0.6813$) because the wrapped configuration allowed for additional pockets of air to form which increased the space between the layers of the FSR, thereby increasing the maximum displacement for force application.

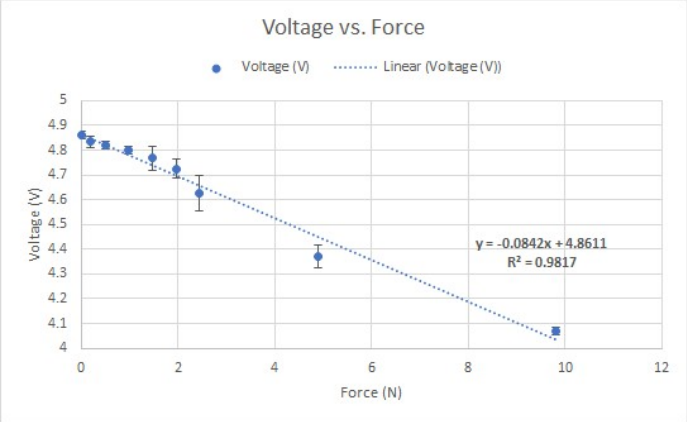

Fig. 6. Voltage versus force calibration curve for the FSR attached to the Cook Aortic Endograft. Known weights were hung on top of the sensor and the voltage outputs were recorded on the y-axis. The curve shows a linear relationship ($R^2 = 0.9817$) between force and voltage.

Comparison to a Commercial Sensor

Next, our FSR attached to a Cook Aortic Endograft was compared to a commercial FSR called a FlexiForce sensor. In order to conduct this comparison, a calibration curve was created for the FlexiForce sensor (Fig. 7). Comparing the FlexiForce's calibration curve to that of the FSR on the Cook Aortic Endograft (Fig. 6), it can be seen that FSR on the Cook Aortic Endograft produces a larger change in voltage in response to force than the FlexiForce sensor.

Using a C-clamp, a constant force was applied to both sensors at the same time and voltages were recorded. The calculated force readings for each of the sensors were determined by inputting the voltage outputs into each sensor's respective calibration curve equation. Fig. 8A shows the average voltage output and standard deviation from five repeated trials for each of the two sensor types. A two tailed Welch's t-test with $\alpha = 0.05$ was performed to determine if the voltage recordings from the FlexiForce sensor and our FSR were significantly different. The t-test determined that there was a significant difference between the voltage readings, with a p value of 0.000137. Because of the difference in responsiveness to force seen in the calibration curves, we suggest that this significant difference between the voltages is due to our FSR being more sensitive to changes in applied force than the FlexiForce sensor. This means that our FSR has greater variation. Fig. 8B shows the average calculated force values and standard deviation from five repeated trials for each of the two sensor types. Running a two-tailed Welch's t-test, on the calculated force values for our FSR's and the FlexiForce showed that there was a

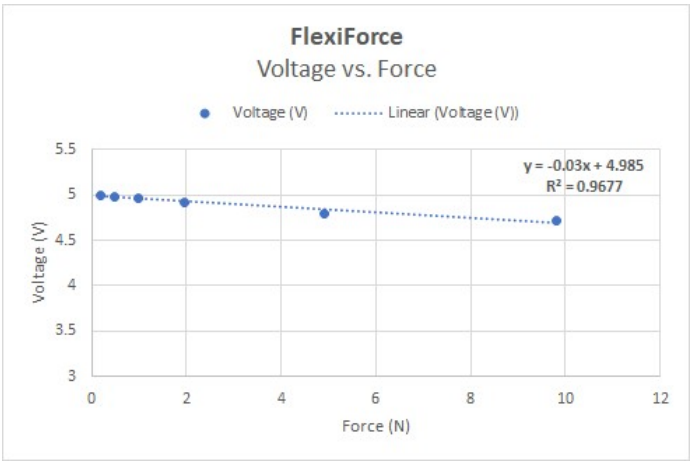

Fig. 7. Voltage versus force calibration curve for the FlexiForce sensor. Known weights were placed on top of the sensor and the voltage outputs were recorded on the y-axis. The curve shows a linear relationship ($R^2 = 0.9677$) between force and voltage.

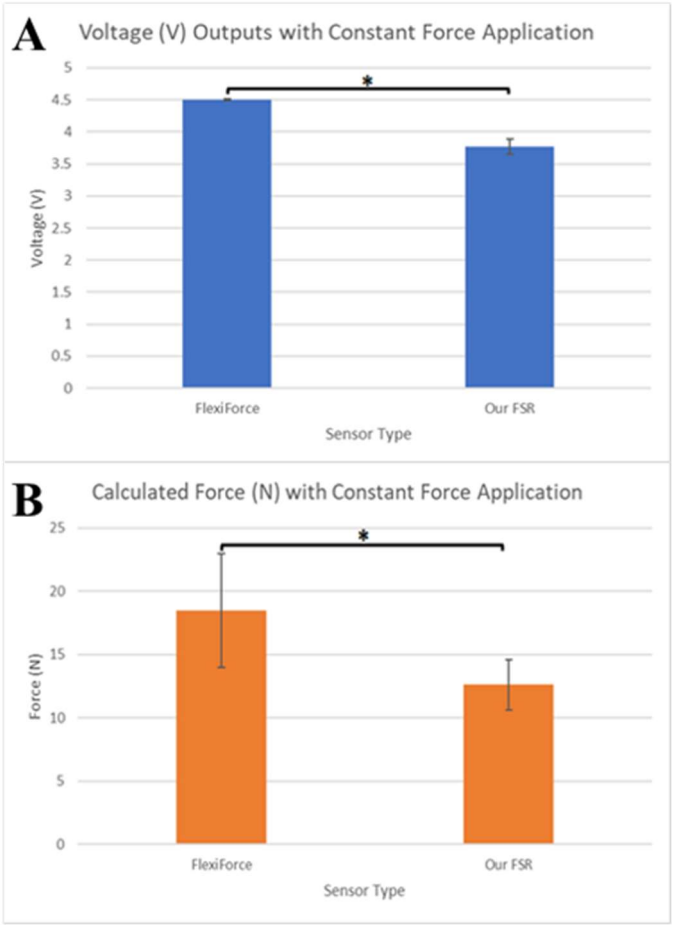

Fig. 8. Average voltage outputs (8A) and calculated force values (8B) for the FlexiForce sensor and our FSR attached to an IR device. A two tailed Welch's t-test with $\alpha = 0.05$ showed a significant difference between the sensors' voltage outputs ($p = 0.000137$) and a significant difference between the sensors' calculated forces ($p = 0.007$).

significant difference (p value = 0.007) between the two sensors' calculated force values. This difference between the sensors' calculated force values could be due to our FSR having a lower precision than the FlexiForce sensor, as suggested by the higher variance in our FSR's voltage readings.

FSR Testing in a Phantom

In order to determine if our FSR device was capable of measuring force applied to a vessel-like structure with elastic properties, the FSR attached to the Cook Aortic Endograft was inserted into the AA phantom and pressed against the wall of the phantom (setup shown in Supplemental Fig. 9). A voltage change was displayed during this force application on the vessel wall. This indicates that our device is capable of measuring forces applied to vessel-like materials. Forces up to 9.8 N were measured inside the phantom. At this force, the phantom did not break even though this is a force that vessels could rupture at. This is most likely due to the higher tensile strain of the phantom material compared to the tensile strain of a human aorta.

Discussion

As the MI device market continues to grow, the need for a force feedback system for these types of devices for these types of devices also increases. Without force feedback, training of experienced clinicians as well as residents and medical students on how to safely navigate a new IR device through a patient's vasculature is limited. If operators exert dangerous levels of force on a vessel wall, rupture can occur and may have devastating effects on the patient. To address this gap in current IR training procedures, we developed an FSR from copper tape, velostat, and double-sided tape that could be attached to IR devices. Our FSR was able to successfully detect both safe and dangerous force values in a vessel-like structure when attached to an IR tool. In addition to being thin and cost efficient, our FSR was also shown to be more sensitive to changes in force compared to a commercially available FSR. These findings suggest that our FSR when attached to a IR device could be a viable teaching tool for training IR clinicians and students in operating devices. Unlike previous force sensing devices, our device is capable of measuring force at the vessel wall in an operator independent fashion. The simple setup of our device also improves upon previous force sensing technology that required time consuming set-up protocols.

Limitations and Future Work

Our current FSR requires further prototyping to address several residual design shortcomings. One flaw in our current FSR design is that after measuring large force values, the FSR requires a recovery period before it can be used again. This recovery period is needed to allow the layers of the sensor materials to return to their original shape. In order to be able to make multiple successive measurements in a training or clinical setting, the layers of the FSR will need to be replaced with materials that have a shorter recovery time. Another deficit in our current FSR design is that while it is highly sensitive to changes in force, it is also imprecise. This would need to be addressed in future work to ensure our FSR is providing consistent information on applied forces. Additionally, our current FSR design only utilizes one sensor on a device. In order to measure force throughout the entire length of a vessel, several sensors would need to be attached to an IR device. Another flaw in our design in its current prototype is that it is not sterilizable. This would be an important factor to address to take the device into clinical testing.

In future research and development of our force sensing tool, it will be important to test the design across multiple IR devices of various sizes. Additionally, phantoms of other vascular structures should be modeled and printed in order to further test the robustness of our device. Future studies may also include the development of a more physiologically accurate material for phantom construction. Additionally, our current force sensing system lacks a user-friendly interface that can easily alert operators when they are applying dangerous levels of force. This should be developed in the future to improve the usability of our device. Lastly, future studies should work to explicitly examine and quantify force direction and magnitude in order to determine the force vectors measured by our device.

Because of the COVID-19 pandemic and restricted lab access, our team was limited in the amount of prototyping and testing that could be conducted on our proposed FSR. With limited lab access, we were also unable to test our FSR in an animal model to determine the effects of a physiological environment on the sensor's ability to detect force. Additionally, the pandemic prevented us from recruiting experienced IR surgeons and residents to test our device in order to gather data on dangerous versus safe force values.

End Matter

Author Contributions and Notes

S.E.D., S.G., and G.A.G. wrote the paper, researched and developed experimental protocols, developed ideas, and collected data. G.A.G. designed and developed the AA and IVC CAD models and aided in final FSR testing. S.E.D. and S.G. prototyped and performed electrical testing and 3D printed the AA model.
The authors declare no conflict of interest.

Acknowledgments

We would like to thank John Angle, M.D. from the U. Va Department of Vascular and Interventional Radiology for advising and funding our research. We would also like to thank William Guilford, Ph.D. from the U.Va Department of Biomedical Engineering for aiding us in the 3D printing process and for allowing us to use his lab and SLA printer.

References

1. General Surgery Devices Market Size, Share & Trends Analysis Report By Application (Orthopedic Surgery, Plastic Surgery), By Type (Medical Robotics & Computer-assisted, Disposable), And Segment Forecasts, 2019 - 2026. *Grand View Research.* https://www.grandviewresearch.com/industry-analysis/general-surgery-devices-market (2019).
2. Gawande, A. A., Zinner, M. J., Studdert, D. M. & Brennan, T. A. Analysis of errors reported by surgeons at three teaching hospitals. *Surgery* **133**, 614–621 (2003).
3. Regenbogen, S. E. *et al.* Patterns of Technical Error Among Surgical Malpractice Claims: An Analysis of Strategies to Prevent Injury to Surgical Patients. *Annals of Surgery* **246**, 705–711 (2007).
4. White, A. *et al.* Inconsistent reporting of minimally invasive surgery errors. *Annals of The Royal College of Surgeons of England* **97**, 608–612 (2015).
5. Rafii-Tari, H. *et al.* Objective Assessment of Endovascular Navigation Skills with Force Sensing. *Ann Biomed Eng* **45**, 1315–1327 (2017).
6. Haraguchi, K. *et al.* A Mechanical Coil Insertion System for Endovascular Coil Embolization of Intracranial Aneurysms. *Interv Neuroradiol* **19**, 159–166 (2013).
7. Force Sensing Resistors - Shunt Mode vs. Thru Mode. Butler Technologies Inc https://butlertechnologies.com/shunt-mode-vs-thru-mode/ (2020).

8. How Does a Force Sensing Resistor (FSR) Work? *Tekscan* https://www.tekscan.com/blog/flexiforce/how-does-force-sensing-resistor-fsr-work (2019).
9. Merten, E. C., Cwik, J. C., Margraf, J. & Schneider, S. Overdiagnosis of mental disorders in children and adolescents (in developed countries). *Child Adolesc Psychiatry Ment Health* **11**, 5 (2017).
10. A, D., Bk, T. & A, B. Study of aortic- common iliac bifurcation and its clinical significance. *J Clin Diagn Res* **8**, AC06-8 (2014).
11. Gameraddin, M. Normal abdominal aorta diameter on abdominal sonography in healthy asymptomatic adults: impact of age and gender. *Journal of Radiation Research and Applied Sciences* **12**, 186–191 (2019).
12. Joh, J. H., Ahn, H.-J. & Park, H.-C. Reference Diameters of the Abdominal Aorta and Iliac Arteries in the Korean Population. *Yonsei Med J* **54**, 48–54 (2013).
13. Li, A. E. *et al.* Using MRI to assess aortic wall thickness in the multiethnic study of atherosclerosis: distribution by race, sex, and age. *AJR Am J Roentgenol* **182**, 593–597 (2004).
14. Prince, M. R., Novelline, R. A., Athanasoulis, C. A. & Simon, M. The diameter of the inferior vena cava and its implications for the use of vena caval filters. *Radiology* **149**, 687–689 (1983).
15. Yang, M., Sun, L., Zhang, J., Li, L. & Yong, J. Diameter and length measurement of infrarenal inferior vena cava in Shandong Peninsula adult and its significance. *Zhonghua Wai Ke Za Zhi* **49**, 514–516 (2011).
16. Oguzkurt, L. *et al.* Computed tomography findings in 10 cases of iliac vein compression (May-Thurner) syndrome. *Eur J Radiol* **55**, 421–425 (2005).
17. Bordei, P., Costin, C., Baz, A., Iliescu, D. & Ionescu, C. Morphometry of the common iliac veins. (2013).
18. Akhgar, J. *et al.* Anatomical Location of the Common Iliac Veins at the Level of the Sacrum: Relationship between Perforation Risk and the Trajectory Angle of the Screw. *Biomed Res Int* **2016**, (2016).
19. Lurie, D. K., Webster, D., Lutz, M., Engle, J. & Shaldenbrand, J. Occlusive vascular stapling in a canine inferior vena cava model. *Journal of Vascular Surgery* **12**, 38–40 (1990).
20. Vorp, D. A. *et al.* Effect of aneurysm on the tensile strength and biomechanical behavior of the ascending thoracic aorta. *The Annals of Thoracic Surgery* **75**, 1210–1214 (2003).
21. Snowhill, P. B. & Silver, F. H. A Mechanical Model of Porcine Vascular Tissues-Part II: Stress–Strain and Mechanical Properties of Juvenile Porcine Blood Vessels. *Cardiovasc Eng* **5**, 157–169 (2005).
22. Using Elastic 50A Resin. *Formlabs* https://support.formlabs.com/s/article/Using-Elastic-Resin?language=en_US (2020).
23. FlexiForce Integration Guides. *Tekscan* https://www.tekscan.com/flexiforce-integration-guides (2016).
24. Yang, C. et al. A vascular interventional surgical robot based on surgeon's operating skills. *Med Biol Eng Comput* **57**, 1999–2010 (2019).
25. Westwood, J. D., Haluck, R. S. & Hoffman, H. M. *Medicine Meets Virtual Reality 13: The Magical Next Becomes the Medical Now*. (IOS Press, 2005).

Supplementary Material:

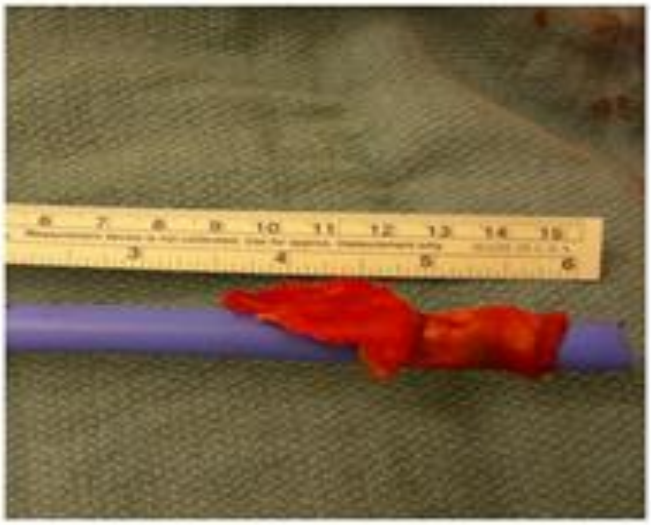

Supplementary Fig. 1. Aortic Section Removed in IR Procedure. Aortic segment removed due to inappropriate amounts of force applied during the procedure.

Supplementary Fig. 3. Force sensor iterations with a flat configuration. Multiple iterations of force sensing resistors in a flat configuration.

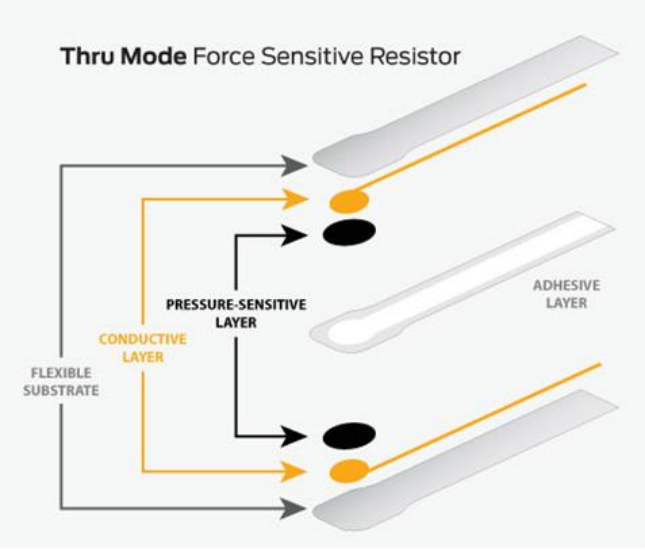

Supplementary Fig. 2. **Layers of a thru mode force sensing resistor.** Layers of a thru mode force sensing resistor. This diagram demonstrates how the conductive layers, pressure sensitive layers, and adhesive layer combine to create an FSR.

Supplementary Fig. 4. CAD model of the aorta and common iliac arteries. This image shows the CAD design for the phantom aorta.

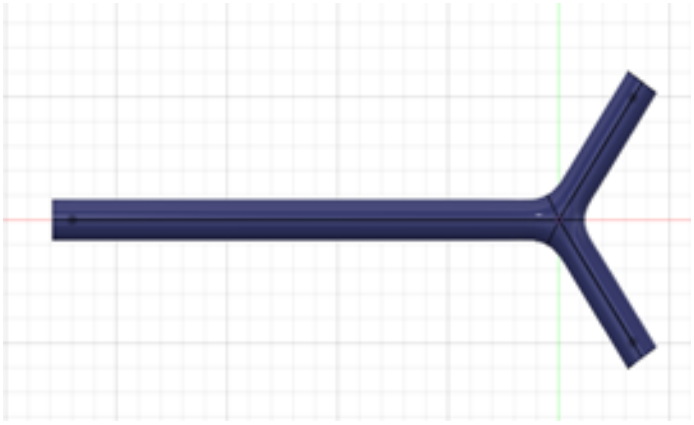

Supplementary Fig. 5. CAD model of the vena cava and common iliac veins. This image shows the CAD design for the phantom vena cava.

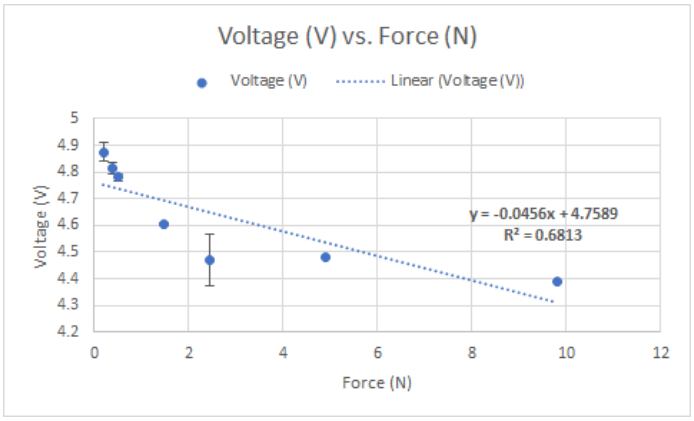

Supplementary Fig. 7. Average voltage of a flattened sensor over the entire range. The sensor has less of a linear relationship but has different voltage responses for safe and unsafe forces.

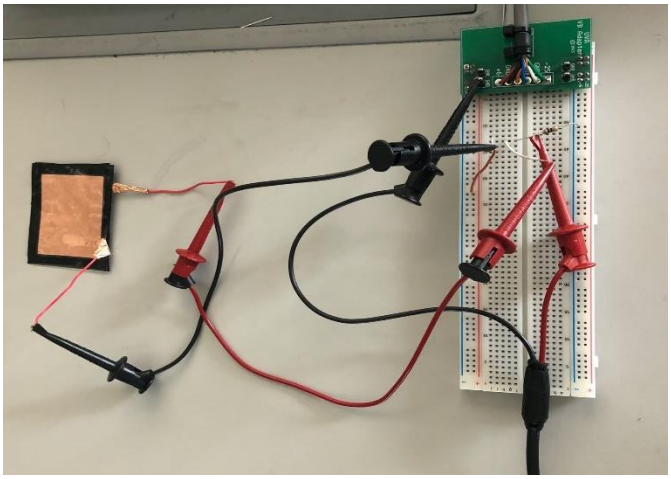

Supplementary Fig. 6. Circuit set-up for calibration of flat sensor. Circuit set-up for calibration of flat sensor. This is a voltage divider circuit, where voltage is measured across the sensor.

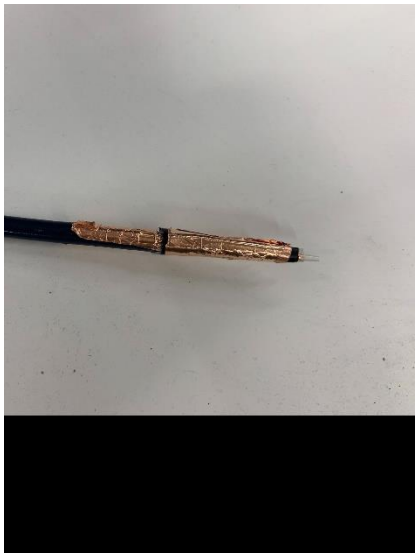

Supplementary Fig. 8. Device prototype. Our FSR placed on an abdominal aortic endograft device.

Supplementary Fig. 9. Phantom device testing set-up.
Experimental set-up for testing functionality in a phantom. Our sensor is wrapped around the Cook aortic endograft device and placed in the phantom. A FlexiForce sensor was also tested inside this phantom.